Searching for Alternatives to Full Kinetic Analysis in ^{18}F-FDG PET: An Extension of the Simplified Kinetic Analysis Method

Sebastien Hapdey[1], Irene Buvat[2], Joan M. Carson[3], Jorge A. Carrasquillo[4], Millie Whatley[3], and Stephen L. Bacharach[5]

[1]Department of Nuclear Medicine, Centre Henri Becquerel and Laboratoire QuantIF-LITIS EA 4108, University of Rouen, Rouen, France; [2]Laboratory of Imaging and Modelling in Neurobiology and Oncology, UMR 8165 CNRS–Paris 7 University–Paris 11 University, Orsay, France; [3]Department of Nuclear Medicine, Clinical Center, National Institutes of Health, Bethesda, Maryland; [4]Department of Radiology, Memorial Sloan-Kettering Cancer Center, New York, New York; and [5]University of California, San Francisco, California

The most accurate way to estimate the glucose metabolic rate (or its influx constant) from ^{18}F-FDG PET is to perform a full kinetic analysis (or its simplified Patlak version), requiring dynamic imaging and the knowledge of arterial activity as a function of time. To avoid invasive arterial blood sampling, a simplified kinetic analysis (SKA) has been proposed, based on blood curves measured from a control group. Here, we extend the SKA by allowing for a greater variety of arterial input function (A(t)) curves among patients than in the original SKA and by accounting for unmetabolized ^{18}F-FDG in the tumor. **Methods:** Ten A(t)s measured in patients were analyzed using a principal-component analysis to derive 2 principal components describing most of the variability of the A(t). The mean distribution volume of ^{18}F-FDG in tumors for these patients was used to estimate the corresponding quantity in other patients. In subsequent patient studies, the A(t) was described as a linear combination of the 2 principal components, for which the 2 scaling factors were obtained from an early and a late venous sample drawn for the patient. The original and extended SKA (ESKA) were assessed using fifty-seven ^{18}F-FDG PET scans with various tumor types and locations and using different injection and acquisition protocols, with the K_i derived from Patlak analysis as a reference. **Results:** ESKA improved the accuracy or precision of the input function (area under the blood curve) for all protocols examined. The mean errors ($\pm$SD) in K_i estimates were $-12\% \pm 33\%$ for SKA and $-7\% \pm 22\%$ for ESKA for a 20-s injection protocol with a 55-min postinjection PET scan, $20\% \pm 42\%$ for SKA and $1\% \pm 29\%$ for ESKA ($P < 0.05$) for a 120-s injection protocol with a 55-min postinjection PET scan, and $-37\% \pm 19\%$ for SKA and $-4\% \pm 6\%$ for ESKA ($P < 0.05$) for a 20-s injection protocol with a 120-min postinjection PET scan. Changes in K_i between the 2 PET scans in the same patients also tended to be estimated more accurately and more precisely with ESKA than with SKA. **Conclusion:** ESKA, compared with SKA, significantly improved the accuracy and precision of K_i estimates in ^{18}F-FDG PET. ESKA is more robust than SKA with respect to various injection and acquisition protocols.

P ET using ^{18}F-FDG is useful for grading tumors and assessing therapy or disease progression (*1,2*). ^{18}F-FDG uptake is often characterized by calculating the standardized uptake value (SUV) from late static imaging (typically 45–60 min after injection). However, SUV is sensitive to body composition (*3*), change in uptake over time (*4*), and blood glucose concentration (*5*), which compromise the use of SUVs for inter- or intrapatient comparison (*6*). Several normalization schemes have been proposed to reduce this sensitivity (*7*) but do not account for variations in ^{18}F-FDG pharmacokinetics among individual patients, and these methods do not differentiate metabolized from unmetabolized ^{18}F-FDG within the tumor. The most accurate way to characterize the glucose metabolic rate is to perform a full kinetic analysis (or its simplified Patlak version (*8*)) to estimate the influx constant (K_i) of ^{18}F-FDG in the tumor. Computing K_i, however, requires dynamic PET to assess the tumor uptake kinetics (tumor uptake at time t [T(t)]) and repeated blood sampling or dynamic imaging over the heart or aorta to measure the arterial input function A(t).

As a compromise between SUV and Patlak analysis, the so-called simplified kinetic analysis (SKA) has been proposed (*7*). In this method, the shape of the patient's A(t) is assumed to follow a mathematic model derived from a group of subjects. For any patient, the A(t) magnitude is obtained by scaling the A(t) model to fit 1 late venous blood sample. A drawback of this approach is that it assumes that a single function can model every individual patient's A(t) after appropriate scaling (*1,7,9*). In addition, SKA does not differentiate metabolized from unmetabolized ^{18}F-FDG in the tumor. To overcome the SKA limitations, we propose an extended SKA method (ESKA), which allows for a greater

variety of A(t) curves among patients and accounts for unmetabolized ^{18}F-FDG in the tumor. We compare the performance of SKA and ESKA, using Patlak analysis as a reference.

MATERIALS AND METHODS

Patlak Analysis

In the Patlak method (8), the K_i of ^{18}F-FDG in the tumor is given by:

$$T(t)/A(t) = K_i \cdot AUC(t)/A(t) + U, \qquad \text{Eq. 1}$$

where U is the steady-state distribution volume of the exchanging compartments (blood and parenchymal tissue) in the tissue region of interest and AUC(t) is the area under the A(t) up to time t, corresponding to the ^{18}F-FDG that has been made available to the tumor up to time t. In this study, A(t) and AUC(t) were determined by dynamic PET over the heart.

SKA

The SKA method initially proposed by Hunter et al. (7) requires 1 static acquisition and 1 venous blood sample collected midway through the static acquisition, approximately 55 min after injection of ^{18}F-FDG. In this approach, A(t) is modeled using a triexponential function:

$$A_{SKA}(t) = A_1 \cdot \exp(-b_1 \cdot t) + A_2 \cdot \exp(-b_2 \cdot t)$$
$$+ A_3 \cdot \exp(-b_3 \cdot t), \qquad \text{Eq. 2}$$

where b_1, b_2, and b_3 are assumed to be identical for all patients and are determined from a set of patients for whom repeated blood sampling was performed. For each individual patient, A_1 and A_2 are computed from the patient's lean body mass and injected dose. A_3 is obtained by fitting the $A_{SKA}(t)$ model to a late blood sample. Equation 2 is then used to compute the area under the A(t) curve up to time t, AUC(t). The SKA K_i index, which estimates the K_i index when using the SKA method, is obtained by dividing the tumor uptake $T(t_{late})$ measured on a late image taken at t_{late} by $AUC(t_{late})$:

$$SKA\ K_i = T(t_{late})/AUC(t_{late}), \qquad \text{Eq. 3}$$

assuming the distribution volume of ^{18}F-FDG (U in Eq. 1) can be neglected.

In our study, we implemented 2 versions of SKA. The first was SKA_{pub}, for which we used the b_i parameters provided in the papers by Hunter et al. (7), Graham et al. (10), and Hoekstra et al. (11), given they were supposed to stay in a narrow range for all patients. The second version was SKA_{opt}, for which we used our own patient studies to derive the b_i parameters, by considering the decreasing part of the true A(t).

In both approaches, $A_1 = A_2$ in Equation 2 and was computed as proposed in the papers by Hunter et al. (7), Graham et al. (10), and Hoekstra et al. (11). The lean body mass equations were $1.07 \times$ weight $- 148 \times$ (weight/height^2) for men and $1.1 \times$ weight $- 120 \times$ (weight/height^2) for women (12). A_3 was computed for each patient, using a late $A(t_{late})$ value, where t_{late} corresponded to the end of the scan.

ESKA

Similar to SKA, ESKA is based on an A(t) model, derived from a training subset of randomly chosen patients for whom the fully sampled A(t) was available.

In ESKA, estimating the A(t) relies on the following 3 steps (Fig. 1):

- Resampling all patients' A(t) from the training set to the same time sampling.
- Analyzing the set of resampled A(t) using a principal-component analysis (PCA). We empirically found that the first 2 principal components ($A_{PCA-1}(t)$ and $A_{PCA-2}(t)$) associated with the largest 2 eigenvalues were sufficient to accurately describe any individual A(t):

$$A_{ESKA}(t) = a_1 \cdot A_{PCA-1}(t) + a_2 \cdot A_{PCA-2}(t), \qquad \text{Eq. 4}$$

where a_1 and a_2 represent patient-dependent coefficients.
- Taking venous blood samples for any patient not in the training set; the a_1 and a_2 coefficients are obtained from 2 samples, $A_{ESKA}(t_1)$ and $A_{ESKA}(t_2)$. $A_{ESKA}(t_1)$ was taken early after injection but late enough to ensure arteriovenous activity equilibrium. $A_{ESKA}(t_2)$ was taken at the end of the scan. These 2 values, along with the $A_{PCA}(t_1)$ and $A_{PCA}(t_2)$ values, yielded a system of 2 equations with 2 unknowns, from which a_1 and a_2 could be derived.

Unlike SKA, ESKA accounts for the unmetabolized ^{18}F-FDG in the tumor. Indeed, a mean distribution volume (U_{mean}) was estimated from the group of patients in the training set (1). For
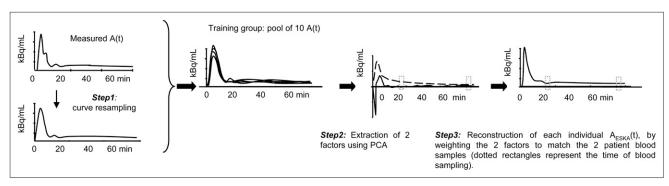

FIGURE 1. Three steps of ESKA approach for estimation of A(t).

each individual patient, the ESKA K_i index, which estimates K_i when using the ESKA method, was then given by:

$$ESKA\ K_i = (T[t_{late}] - U_{mean} \cdot AESKA[t_{late}])/AUC(t_{late}),$$
Eq. 5

for t_{late} corresponding to a late static scan.

Patients

Forty-three patients were considered and divided into 3 groups. Each group corresponded to a particular injection and acquisition protocol, to assess the robustness of the method for various injection durations and delays between injection and scanning. Nineteen patients were studied multiple times (baseline followed by 1 or 2 follow-up studies), resulting in 70 studies, each with the complete A(t) available for reference (Table 1). Pre- and posttherapy scans were combined to compare the various kinetic analysis methods.

Results from the first 2 groups assessed the robustness of the methods to the injection protocol:

- The 120-s/55-m$_{Tot}$ group (33 studies) included 16 patients (47.1 ± 13.7 y) with renal cell cancer receiving vascular endothelial growth factor antibody. Each patient underwent a 120-s ^{18}F-FDG injection protocol using a constant-infusion pump. These patients were scanned dynamically for about 55 min after injection.
- The 20-s/55-m$_{Tot}$ group (37 studies) included 27 patients (47.6 ± 17.3 y) who underwent a 20-s ^{18}F-FDG injection protocol using a constant-infusion pump. These patients were enrolled in 3 different protocols: 13 breast cancer patients were receiving anti–epidermal growth factor receptor therapy, 7 patients with various tumor locations were receiving various types of antineoplastic therapy, and 7 patients were admitted for diagnosis of lymph node lesions. These patients were scanned dynamically for approximately 55 min after injection.
- To investigate the robustness of the methods regarding the delay between injection and scanning, another group was derived from the 20-s/55-m group, considering delayed data:
- The 20-s/120-m$_{Tot}$ group (7 studies) included the 7 patients from the 20-s/55-m$_{Tot}$ group (25.7 ± 13.3 y) presenting

lymph node inflammation for whom we had a delayed whole-body scan available. This delayed whole-body scan allowed assessment of the tumor at 1 additional late time point, approximately 90–150 min after injection depending on the lesion localization. In this group, we considered tumors only with stable Patlak K_i—that is, with K_i that did not vary by more than 15% between the injection groups at 55 and 120 min.

Patient Training and Testing Groups. To derive the A(t) models (SKA parameter b_i and the 2 principal components $A_{PCA-1}(t)$ and $A_{PCA-2}(t)$ needed for ESKA), some of the patients from the 120-s/55-m$_{Tot}$ and 20-s/55-m$_{Tot}$ groups were removed to be used as a training set. The training subjects used for computing these parameters or principal components were not further included in the analyses. The same training subjects were used for SKA and ESKA. Thus, in the testing set, 10 subjects were in the 120-s/55-m, 21 in the 20-s/55-m, and 7 in the 20-s/120-m groups (Table 1).

We also used pairs of successive PET/CT scans acquired in the same subjects to study the accuracy and precision in measuring changes in K_i between 2 PET/CT scans (ΔK_i). After removal of the cases used in the training set, we had 13 tumors for which ΔK_i between 2 scans was available in the 20-s/55-m group and 31 tumors in the 120-s/55-m group, with an average time lapse between the 2 scans of 34.6 ± 14.8 and 42.5 ± 10.0 d, respectively (none in the 20-s/120-m group).

Lesions Considered in Study. The field of view explored on the first PET scan was chosen to include lesions greater than 2 cm in their longest dimension based on CT or MRI data. All additional lesions in the field of view at the time of the first dynamic PET scan were also considered. Overall, a total of 124 lesions were investigated.

Patient Dose. For each patient, approximately 370 MBq (379 ± 61 MBq) of ^{18}F-FDG were injected, except for the 7 patients with lymphatic lesions (560.1 ± 14.8 MBq for the 4 adults and 201.5 ± 75.4 MBq for the 3 children).

Data Acquisition

For all patients, ^{18}F-FDG PET studies were acquired dynamically, starting at injection time, on an Advance PET (GE

TABLE 1
Patient Population

Group		Population description	No. of studies (=no. of A(t))	No. of lesions
120 s/55 m	Training	6 patients with renal cell cancer (5 men, 1 woman; mean age ± SD, 52.3 ± 9.5 y)	10	
	Test	10 patients with renal cell cancer (9 men, 1 woman; mean age ± SD, 44 ± 15 y)	23	51
20 s/55 m	Training	3 patients with breast cancer (mean age ± SD, 60.7 ± 13.3 y)	10	
		3 patients, 1 with breast and 2 with ovarian cancers (mean age ± SD, 52.3 ± 5.5 y)		
	Test	10 patients with breast cancer (mean age ± SD, 53.9 ± 9.8 y)	27	65
		4 patients, 1 with breast, 2 with ovarian, and 1 with prostate cancers (1 man, 3 women; mean age ± SD, 54.7 ± 11.9 y)		
		7 patients with lymph node lesions (2 men, 5 women; mean age ± SD, 25.7 ± 13.3 y)		
20 s/120 m	Test	7 patients with lymph node lesions (2 men, 5 women; mean age ± SD, 25.7 ± 13.3 y)	7	8

Healthcare) scanner in 2-dimensional mode, producing 35 slices over a 15-cm axial field of view.

For the 120-s injection protocol (the 120-s/55-m group), the time per frame was 30 s (0–4 min after injection), 3 min (4–40 min after injection), and 5 min thereafter, for an average of 51.3 ± 2.2 min scan time.

For the 20-s injection protocol (the 20-s/55-m and 20-s/120-m groups), the time per frame was 5 s (0–1 min after injection), 15 s (1–2 min after injection), 30 s (2–7 min after injection), 3 min (7–25 min after injection), and 5 min thereafter, for an average of 54.7 ± 1.1 min scan time.

When tumors were not at the level of the heart (17 studies in total), the scan was started over the heart for a period of approximately 25 min and then shifted to the tumor level for the remaining dynamic acquisition time.

A static image at the tumor level was systematically computed from the dynamic acquisition, summing the last 3 acquisition time points (~45–60 min after injection).

In addition to the dynamic acquisition, the 7 patients in the 20-s/120-m group underwent a whole-body static acquisition at the end of the dynamic acquisition, on which the node and heart uptake was seen at the late time point (between 90 and 150 min, depending on the number of steps before reaching the tumor location, step duration, scan starting time). The time associated with the node (or the heart) level was computed from the whole-body starting time and the slice including the node (or the heart).

Data Processing

Image Reconstruction. Images were reconstructed at 2 mm/pixel into a 256×256 matrix using ordered-subset expectation maximization (4 iterations, 28 subsets, 5-mm gaussian postreconstruction filtering) including attenuation, scatter, random, dead time, and decay corrections. The reconstructed images had a transaxial and axial resolution of approximately 7 mm.

Input Function. The A(t)s were needed for Patlak analysis, which was used as the reference method against which we compared SKA and ESKA. If the tumors were at the level of the heart, A(t) was directly derived from the dynamic images by placing a volume of interest manually in the left atrial cavity (as visualized from the sum of the early arterial phase dynamic images), because this structure is less affected by activity spillover from atrial muscle than the left ventricle cavity, which can be strongly affected by spillover from the myocardium. When the tumor was not at the level of the heart, A(t) was also estimated from the images for the first 25 min (because the first 25 min of data were always acquired at the level of the heart). Then, when the scanner was moved to the level of the tumor, the later A(t) time points were obtained from blood samples taken approximately every 5 min thereafter.

In the Patlak analysis, the data from 25 min after injection to the end of acquisitions were used to obtain the slope K_i and the distribution volume U.

In SKA and ESKA, the input function was estimated using t_{late} (~55 min for the 20-s/55-m and 120-s/55-m groups and ~120 min for the 20-s/120-m group).

Volumes of Interest. Volumes of interest were drawn over the tumors on each patient from the late tumor static scan using an automatic 3-dimensional region-growing program based on a threshold in uptake (i.e., a percentage of maximum voxel intensity) as implemented in the MedX software (Sensors System). These volumes of interest were used for calculation of the SKA K_i and ESKA K_i values and the Patlak K_i. For the whole-body images, we computed the tumor volumes of interest with the same 3-dimensional region-growing program, using the same tumor uptake threshold as when using dynamic images.

Data Analysis

Performances of SKA_{pub}, SKA_{opt}, and ESKA were assessed by comparing the estimated A(t) with the PET image–derived A(t). A percentage error between the estimated area under the curve (AUC) and the AUC derived from the continually sampled A(t) was calculated.

SKA_{pub} K_i, SKA_{opt} K_i, and ESKA K_i were compared with our gold standard Patlak K_i using correlation analyses and percentage errors. Estimated ΔK_i based on estimated K_i from SKA_{pub}, SKA_{opt}, and ESKA were also compared with ΔK_i based on Patlak K_i, to study the accuracy and precision in measuring changes in K_i.

Averaged percentage errors, with the percentage error defined by $100 \times$ (estimated_value − reference_value)/reference_value, and associated variance were compared using the nonparametric Wilcoxon matched-pairs signed-rank test and Friedman test, respectively, with an $\alpha = 0.05$ level of significance. Statistical difference of the nonparametric Spearman correlation coefficients was computed using the Fisher r-to-Z transformation.

RESULTS

We first evaluated the methods for the 120-s/55-m and 20-s/55-m groups, corresponding to acquisitions of about 55 min obtained using two ^{18}F-FDG infusion protocols. We then tested the robustness of the 3 methods for the delayed imaging protocol.

A(t) and AUC Estimates

Figure 2 shows the A(t) (first 10 min only), obtained using SKA_{pub}, SKA_{opt}, and ESKA, compared with the reference A(t) for the training and test subsets of the 20-s/55-m group. Large differences between estimated and true A(t) can be seen with SKA_{pub}. This result was expected because SKA was not meant to reproduce the shape of the A(t)s at early times. However, a good agreement between the estimated A(t) and the reference A(t) was observed with both SKA_{opt} and ESKA.

Table 2 gives the percentage errors in AUC estimated for SKA_{pub}, SKA_{opt}, and ESKA, compared with the reference AUC and the correlation coefficients between reference and estimated AUC. With ESKA, the maximum error in AUC estimate for the 120-s/55-m and 20-s/55-m groups was 8.4%, and the mean error was $-0.3\% \pm 4.3\%$ (computing a combined error for the 2 groups). For these same groups, the maximum error reached 193.8% and 56.7% for SKA_{pub} and SKA_{opt}, respectively, and the combined-group mean errors were $52.9\% \pm 45.2\%$ and $9.1\% \pm 15.0\%$, respectively. The correlation coefficients for ESKA were always significantly higher than the ones obtained for the SKA approaches.

The trends for the 20-s/120-m group were the same as those observed for the 120-s/55-m and 20-s/55-m groups. SKA_{pub} resulted in the largest AUC overestimation for all groups. The decrease in the mean percentage error between
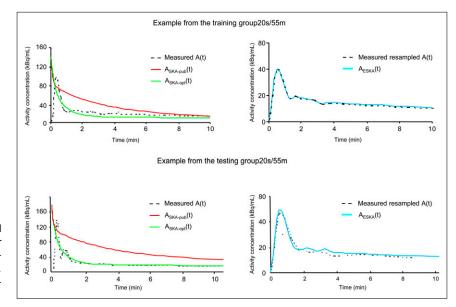
FIGURE 2. (Left) Comparison of original A(t) (first 10 min) with SKA method of Hunter et al. (7), using both published and optimized parameter values to compute $A_{SKA}(t)$. (Right) For same patient studies, comparison of $A_{ESKA}(t)$ with original resampled A(t).

SKA_{pub} and SKA_{opt} and the decrease in the mean percentage error between SKA_{opt} and ESKA were statistically significant. The correlation coefficient was significantly higher for ESKA than for SKA_{opt} and SKA_{pub}, except for the 20-s/120-m group (possibly because of the low number of subjects in that group). For all methods, except again for the 20-s/120-m group, the magnitude of the error in AUC estimate was not correlated with the magnitude of the reference AUC (results not shown).

K_i Estimates

Table 3 presents the mean percentage error in the estimation of the Patlak K_i for the 3 approaches and the r^2 values between estimated and reference K_i. Although the AUC estimates were more accurate for SKA_{opt} than for SKA_{pub} (Table 2), the K_i values from SKA_{opt} were significantly less accurate than the K_i values from SKA_{pub}. K_i estimates were the most accurate with ESKA, although the percentage errors were highly variable. To test whether the large SD of errors for ESKA was due to using a single U_{mean} to estimate the ^{18}F-FDG distribution volume, we used the true tumor's distribution volume (U_{true}) of ^{18}F-

FDG computed from the Patlak analysis with the known T(t) and A(t) (results not shown). When accounting for U_{true} in ESKA, the SD associated with the mean percentage error in K_i estimates was strongly reduced (mean errors of $-6.4\% \pm 15.2\%$ and $0.9\% \pm 4.9\%$ for the 120-s/55-m and 20-s/55-m groups, respectively). The impact on the error induced by the use of a unique U_{mean} was statistically significant ($P < 0.05$) only for the 20-s/55-m group. U_{true} values ranged from 0.1 to 0.9 vs. 0.5 for the U_{mean} value.

In the 20-s/120-m group, ESKA also resulted in a statistically better estimate of K_i than did SKA ($P < 0.05$), associated with a lower SD ($P < 0.05$ for SKA_{pub} vs. ESKA and for SKA_{opt} vs. ESKA).

For all methods, the magnitude of the error in K_i estimate was not correlated with the magnitude of the reference K_i (results not shown).

The correlation coefficients between the reference and estimated K_i with the SKA methods were similar to or significantly lower than those with the ESKA methods. The ESKA K_i values were more strongly correlated with the Patlak K_i values for the delayed acquisitions than for the 55-min acquisitions ($P < 0.05$ for the 120-s/55-m vs.

TABLE 2
Mean Percentage Differences (±SD) Between Estimated and True AUC and Spearman Correlation for SKA and ESKA

Group	SKA_{pub} Mean ± SD	r^2	SKA_{opt} Mean ± SD	r^2	ESKA Mean ± SD	r^2
20 s/55 m (n = 27)	71.4* ± 53.6%†	0.89	2.5% ± 11.9%	0.71	−0.4% ± 4.1%	0.98‡
20 s/120 m (n = 7)	82.0* ± 41.2%†	0.96	72.5* ± 43.8%†	0.93	6.3* ± 3.2%†	0.96
120 s/55 m (n = 23)	31.2* ± 15.4%†	0.62	16.9* ± 14.6%†	0.64	−0.2* ± 4.6%†	0.93‡

*Results for approach significantly different from those of other 2 in terms of mean (Wilcoxon test).
†Results for approach significantly different from those of other 2 in terms of variance (Friedman test).
‡Results for approach significantly different from other 2 in terms of correlation (Fisher r-to-Z transformation).
All AUCs were computed as area from t = 0 to midpoint of static image.

TABLE 3
Mean Percentage Differences (±SD) Between Estimated K_i and Patlak K_i and Spearman Correlation for SKA and ESKA

Group	SKA$_{pub}$ Mean ± SD	r^2	SKA$_{opt}$ Mean ± SD	r^2	ESKA Mean ± SD	r^2	SKA$_{pub}$ with unmetabolized ^{18}F-FDG* Mean ± SD	r^2	SKA$_{opt}$ with unmetabolized ^{18}F-FDG* Mean ± SD	r^2	ESKA without unmetabolized ^{18}F-FDG* Mean ± SD	r^2
20 s/55 m (n = 65)	−12% ± 33%	0.82†	33‡ ± 36%§	0.93†	−7% ± 22%	0.98†	−40% ± 24%	0.86	−9% ± 22%	0.97	36% ± 33%	0.98
20 s/120 m (n = 8)	−37‡ ± 19%§	0.93	−36‡ ± 20%§	0.93	−4‡ ± 6%§	1.0†	−47% ± 15%	0.93	−46% ± 16%	0.93	13% ± 6%	1.0
120 s/55 m (n = 51)	20‡ ± 42%§	0.94	35‡ ± 47%§	0.94	1‡ ± 29%§	0.93	−22% ± 20%	0.94	−13% ± 22%	0.93	58% ± 65%	0.93

*Results using modifications of 3 methods (SKA$_{pub}$ and SKA$_{opt}$ accounting for U$_{mean}$ or ESKA with U$_{mean}$ set to 0).
†Results for approach significantly different from other 2 in terms of correlation (Fisher r-to-Z transformation).
‡Results for approach significantly different from those of other 2 in terms of mean (Wilcoxon test).
§Results for approach significantly different from those of other 2 in terms of variance (Friedman test).

20-s/120-m groups and for the 20-s/55-m vs. 20-s/120-m groups).

ΔK_i Estimates

Table 4 shows the relative errors (estimated_ΔK_i − Patlak_ΔK_i)/Patlak_ΔK_i when ΔK_i was calculated on the basis of SKA$_{pub}$, SKA$_{opt}$, and ESKA K_i estimates for the 20-s/55-m and 120-s/55-m groups (no data available for the 20-s/120-m group). The smallest mean errors in ΔK_i were obtained with ESKA, followed by SKA$_{opt}$ and then SKA$_{pub}$. The errors were always highly variable (SD > 100%), but the smallest variability was observed with ESKA. The magnitude of the error in ΔK_i estimate was not correlated with the magnitude of the reference ΔK_i (results not shown).

DISCUSSION

In ^{18}F-FDG PET, the glucose metabolic rate is related to the net rate of ^{18}F-FDG influx K_i, which can be estimated using a full kinetic analysis and a measurement of the A(t) or using a Patlak analysis (8). However, full kinetic analysis and Patlak analysis are rarely used in clinical practice because of the time-consuming, full dynamic acquisition protocol they involve. In clinical practice, glucose metabolic rate is usually replaced with the SUV, because use of SUVs requires only 1 late image acquisition. Freedman et al. (1) showed that different conclusions could be reached regarding tumor follow-up depending on whether SUV or Patlak analysis was used.

SKAs differ in the method used to estimate the amount of ^{18}F-FDG delivered to the tumor. The SKA proposed by Hunter et al. (7) uses a single parametric expression for A(t) for all patients and a single blood sample to scale the curve for each subject. Adaptation to different infusion protocols or to different patient populations is only through adjustment of the exponential parameters (as in our SKA$_{opt}$) and by scaling the resulting A(t) using the single blood sample, to correctly estimate the AUC. The A(t) shape actually depends on the injection rate and on the patient's metabolic status. In SKA, this variability is considered using only the scaling factor associated with the third exponential function of the model (Eq. 2). The injection phase is thus neglected, unlike in our ESKA approach. Nor does SKA attempt to account for unmetabolized ^{18}F-FDG in tumor. Sundaram et al. (9) proposed a hybrid model between the SKA method proposed by Hunter et al. (7) and Patlak analysis, using multiple blood samples to account for unmetabolized ^{18}F-FDG. However, only 1 blood sample (40 min after injection) was used to scale each individual patient's A(t). Another approach has been proposed to estimate A(t) using a triexponential function (13) for Na[18]F-PET data. The authors (13) reported a good correlation between true and estimated A(t) but used the same population of patients to determine the model parameters and validate the model.

Other groups used image-derived input functions without scaling (14,15), an approach limited by the PET image

TABLE 4
Percentage Errors in Estimation of Change in K_i Between 2 Successive PET/CT Scans When Using SKA_{pub}, SKA_{opt}, or ESKA K_i Estimates

Group	SKA_{pub}	SKA_{opt}	ESKA
20 s/55 m (n = 13)	−135.6* ± 181.3%[†]	31.2% ± 131.5%	0.7% ± 103.8%
120 s/55 m (n = 31)	−123.5% ± 622.1%	−95.4% ± 535.1%[†]	−52.3% ± 212.0%

*In 20-s/55-m group, SKA_{pub} was significantly different from 2 other approaches in terms of mean error. In 120-s/55-m group, mean error was only significantly different between SKA_{pub} and SKA_{opt} (Wilcoxon test).

[†]In 20-s/55-m group, SKA_{pub} was significantly different from 2 other approaches in terms of associated variance. Also, variance of SKA_{opt} was significantly different from that of SKA_{pub} and ESKA (Friedman test).

Data are mean ± SD.

partial-volume effect and radiolabel uptake in tissue surrounding the region of interest.

In this paper, we first considered an approach that optimizes the model parameters for each injection protocol—an alternative version of the SKA method proposed by Hunter et al. (7). Our approach might be more appropriate than the original SKA method when the injection protocol varies. We also derived an alternative model for A(t), with 2 principal components derived from the PCA of a subset of fully sampled A(t) measured using a specific injection protocol. We found (results not shown) that considering more principal components increased variability without reducing error in AUC estimates. Naganawa et al. (16) used independent component analysis to estimate the A(t), along with the tissue time–activity curve, directly from dynamic brain PET series. To deal with the nonunique solution of independent component analysis, these authors introduced anatomic constraints specific to cerebral physiology, which are difficult to adapt in an oncology situation. Their method has the advantage of being independent of the injection protocol and image time sampling and not requiring any manual delineation of the arterial region of interest (16). However, an arterial blood sample was required to scale the estimated input function.

ESKA requires 2 venous blood samples rather than the single sample required by SKA. We do not consider this requirement a significant drawback, because once the patient has a venous line in place to draw the 1 sample required by SKA, it is simple to acquire an additional sample later. To improve the robustness of the fit, 1 early and 1 late sample are required. The first blood sample should be drawn as soon as possible after equilibration between arterial and venous blood has been reached, to accurately estimate the early part of the A(t). From visual examination of the A(t) of the training sets, we chose to draw our first sample at approximately 15 min after injection for the 120-s injection protocol and approximately 10 min after injection for the 20-s injection protocol. Neither the SKA nor the ESKA methods require dynamic imaging. Only a single, late static image is necessary.

Another advantage of the ESKA method is that unlike SKA, ESKA attempts to account for the presence of unmetabolized ^{18}F-FDG when deriving the K_i, based on the average distribution volume of ^{18}F-FDG observed in the training set.

A(t) and AUC Estimates

As illustrated in Figure 2, the A(t) curves recovered using ESKA agree well with the original A(t). ESKA yielded both a better estimate of the AUC and a better correlation with the true AUC than did SKA, for all groups (Table 2).

K_i Estimates

For the 120-s/55-m group, our correlations between SKA K_i and Patlak K_i are consistent with values reported elsewhere in the literature (7,9,10). We found an r^2 coefficient between SKA_{pub} and true K_i of 0.91, whereas previous correlations of 0.89 (10), 0.92 (9), and 0.98 (7) have been reported. However, this high correlation is accompanied by an overestimation of the SKA_{pub} K_i indices similar to that reported by Hunter et al. (7) (although Sundaram et al. (9) reported a 20% underestimation of K_i when using the approach of Hunter et al.).

For the 20-s/55-m group, true K_i and SKA_{pub} K_i agreed less well ($r^2 = 0.59$), although there was only a small underestimation of the SKA_{pub} K_i index, underlining the variability in SKA performance as a function of the injection protocol. SKA_{pub} K_i correlated slightly better with Patlak K_i for 120-min acquisitions than for 55-min acquisitions (Table 3).

There was excellent correlation between Patlak K_i and ESKA K_i for both 20-s and 120-s injections ($r^2 \geq 0.92$). The mean error in K_i with ESKA was also small for both injection protocols, compared with SKA_{opt} (Table 3). To clarify whether the improvement in K_i estimates observed with ESKA was mostly due to better A(t) estimate or to accounting for unmetabolized ^{18}F-FDG, we calculated the mean error in K_i estimates using SKA_{pub} and SKA_{opt} with U set to U_{mean} (as in ESKA) and using ESKA with $U_{mean} = 0$ (Table 3). Table 3 demonstrates that the 2 original features of ESKA (original A(t) estimate and accounting for U_{mean}) are needed to make ESKA accurate, whatever the injection protocol and acquisition time, and that SKA cannot perform as well as ESKA, even when accounting for unmetabolized ^{18}F-FDG. With ESKA, a residual error was still observed due to the use of a mean U_{mean} value. Error was reduced in

the 120-min acquisitions, compared with 55-min acquisitions, presumably because of the decrease of unmetabolized ^{18}F-FDG with time. Also, the SD associated with the mean error was reduced to 6.2% (20-s/120-m group), compared with 28.8% and 22.4% for the 120-s/55-m and 20-s/55-m groups, respectively ($P < 0.05$).

Compared with ESKA, the larger SD in the SKA methods was due to not accounting for unmetabolized ^{18}F-FDG, as demonstrated in Table 3, in which the SD systematically decreased when U_{mean} was included in the SKA methods.

SKA$_{pub}$ Versus SKA$_{opt}$

In all our patient groups, the AUC was overestimated using SKA$_{pub}$. The results in Figure 2 show the need to adapt the parameters to the injection protocol if the objective is to estimate the A(t) shape accurately. However, even when optimizing the SKA parameters for our injection protocols, SKA still resulted in an AUC overestimation, probably because a single AUC shape, even scaled, cannot be appropriate for every patient. Using SKA$_{opt}$ instead of SKA$_{pub}$ left the correlation with true K_i unchanged or improved the correlation, but it did not necessarily improve the K_i estimates, because with SKA$_{pub}$ the underestimation of K_i due to the overestimation of AUC is partially compensated by not accounting for unmetabolized ^{18}F-FDG (i.e., overestimating K_i).

ΔK$_i$ Estimates

Results in Table 4 show that ESKA tends to estimate ΔK_i more accurately and more precisely than SKA, demonstrating that the reduction of bias in K_i estimates obtained using ESKA is not at the expense of increased variability. These results are consistent with the correlation results shown in Table 3 and suggest that ESKA might be preferable to SKA when using K_i for patient monitoring.

Limitations of ESKA

A source of A(t) variability is the time lag between the start of the scanning and the arrival of activity in the field of view. To remove such variability and correctly align the A(t) peak time in ESKA, we aligned the original A(t)s during the resampling step so that each A(t) peaked at the same time point. This realignment can be done a posteriori, as we did here, or by synchronizing the scanning start time with the detection of activity in the field of view.

In ESKA, the unmetabolized ^{18}F-FDG in the tumor is accounted for using the U_{mean} obtained from the training set from each population (Eq. 5). However, only a true kinetic analysis could determine the exact distribution volume. Using only a mean value may cause variability in K_i, as previously reported (1). Variability in tumor distribution volume likely reflects real variations in tumor viable cell density, edema, and other factors that are hard to predict on the basis of other observables—that is, tumor or background uptake, input function, patient weight, and K_i estimate. Note that delayed imaging protocols (e.g., 120 min after injection or longer) have recently proven of clinical interest (17–19). Because unmetabolized ^{18}F-FDG is usu-

ally quite low in these cases, the errors in estimating unmetabolized ^{18}F-FDG by ESKA should be less important.

CONCLUSION

By accounting for variability in the shape of A(t) using 2 venous blood samples and partially accounting for unmetabolized ^{18}F-FDG in the tumors, the ESKA approach proposed here yields significantly more accurate and more precise estimates of the net ^{18}F-FDG K_i than those achieved with the conventional SKA. These improvements also translate into more accurate estimates of changes in K_i over time.

DISCLOSURE STATEMENT

REFERENCES

1. Freedman N, Sundaram SK, Kurdziel K, et al. Comparison of SUV and Patlak slope for monitoring of cancer therapy using serial PET scans. *Eur J Nucl Med.* 2003;30:46–53.
2. Romer W, Hanauske AR, Ziegler S, et al. Positron emission tomography in non-Hodgkin's lymphoma: assessment of chemotherapy with fluorodeoxyglucose. *Blood.* 1998;91:4464–4471.
3. Zasadny KR, Wahl RL. Standardized uptake values of normal tissues at PET with 2-[fluorine-18]-fluoro-2-deoxy-D-glucose: variations with body weight and method for correction. *Radiology.* 1993;189:847–850.
4. Hamberg LM, Hunter GJ, Alpert NM, Choi NC, Babich JW, Fischman AJ. The dose uptake ratio as an index of glucose metabolism: useful parameter or oversimplification? *J Nucl Med.* 1994;35:1308–1312.
5. Lindholm P, Minn H, Leskinen-Kallio S, Bergman J, Ruotsalainen U, Joensuu H. Influence of blood glucose concentration on FDG uptake in cancer: a PET study. *J Nucl Med.* 1993;34:1–6.
6. Kim CK, Gupta NC, Chandramouli B, Alavi A. Standardized uptake values of FDG: body surface area is preferable to body weight. *J Nucl Med.* 1994;35:164–167.
7. Hunter GJ, Hamberg LM, Alpert NM, Choi NC, Fischman AJ. Simplified measurement of deoxyglucose utilization rate. *J Nucl Med.* 1996;37:950–955.
8. Patlak CS, Blasberg RG, Fenstermacher JD. Graphical evaluation of blood-to-brain transfer constants from multiple-time uptake data. *J Cereb Blood Flow Metab.* 1983;3:1–7.
9. Sundaram SK, Freedman NM, Carrasquillo JA, et al. Simplified kinetic analysis of tumor ^{18}F-FDG uptake: a dynamic approach. *J Nucl Med.* 2004;45:1328–1333.
10. Graham MM, Peterson LM, Hayward RM. Comparison of simplified quantitative analyses of FDG uptake. *Nucl Med Biol.* 2000;27:647–655.
11. Hoekstra CJ, Paglianiti I, Hoekstra OS, et al. Monitoring response to therapy in cancer using [^{18}F]-2-fluoro-2-deoxy-D-glucose and positron emission tomography: an overview of different analytical methods. *Eur J Nucl Med.* 2000;27:731–743.
12. Morgan DJ, Bray KM. Lean body mass as a predictor of drug dosage: implications for drug therapy. *Clin Pharmacokinet.* 1994;26:292–307.
13. Hirata T, Wakita K, Fujioka M, et al. Reliability of one-point blood sampling method for calculating input function in NaF18 PET. *Nucl Med Commun.* 2005;26:519–525.
14. Geus-Oei LF, Visser EP, Krabbe PF, et al. Comparison of image-derived and arterial input functions for estimating the rate of glucose metabolism in therapy-monitoring ^{18}F-FDG PET studies. *J Nucl Med.* 2006;47:945–949.
15. Zanotti-Fregonara P, Fadaili EM, Maroy R, et al. Comparison of eight methods for the estimation of the image-derived input function in dynamic [^{18}F]-FDG PET human brain studies. *J Cereb Blood Flow Metab.* 2009;29:1825–1835.
16. Naganawa M, Kimura Y, Ishii K, Oda K, Ishiwata K, Matani A. Extraction of a plasma time-activity curve from dynamic brain PET images based on independent component analysis. *IEEE Trans Biomed Eng.* 2005;52:201–210.
17. Boerner AR, Weckesser M, Herzog H, et al. Optimal scan time for fluorine-18 fluorodeoxyglucose positron emission tomography in breast cancer. *Eur J Nucl Med.* 1999;26:226–230.
18. Kubota K, Itoh M, Osaki K, et al. Advantage of delayed whole-body FDG-PET imaging for tumor detection. *Eur J Nucl Med.* 2001;28:696–703.
19. Nakamoto Y, Higashi T, Sakahara H, et al. Delayed ^{18}F-fluoro-2-deoxy-D-glucose positron emission tomography scan for differentiation between malignant and benign lesions in the pancreas. *Cancer.* 2000;89:2547–2554.